(ISSN: 0973-7049(P))

The Bioscan AN INTERNATIONAL QUARTERLY JOURNAL OF LIFE SCIENCES 21(3, 845-853, 2026 www.thebioscan.com

Crystals Based on Alkali and Alkaline Earth Metal Halides: An Overview

N. Manonmani

Associate Professor, Department of Chemistry, Government Arts and Science College, Palkulam, Kanyakumari-629401, Affiliated to Manonmaniam Sundaranar University, Abishekkapatti, Tirunelveli, Tamil Nadu, India

Email: manosushmi@gmail.com

ORCID: 0000-0003-0854-8938

DOI: https://doi.org/10.63001/tbs.2026.v21.i03.pp845-853

KEYWORDS

Inorganic materials, Ionic conductors, Alkali and alkaline earth metal halides, Crystal growth from solution, Physico-chemical properties, Solid-state batteries.

Article Info

Received: 08.07.2026

Accepted: 14.08.2026

Published: 09.09.2026

Abstract

Single crystals belonging to the $A_3MX_5 \cdot 2H_2O$ family (where A = alkali metal, M = alkaline earth metal, and X = halogen) possess exceptionally interesting optical and electrical properties. However, their structurally incommensurate nature has historically impeded precise X-ray crystal structure refinements. Introducing intentional non-stoichiometry into such incommensurate structures offers a promising pathway toward engineering novel ionic-conducting single crystals tailored for solid-state batteries and next-generation energy storage applications.

In this work, single crystals of non-stoichiometric sodium calcium chloride hydrate, $Na_3CaCl_5 \cdot 2H_2O$, were successfully grown from aqueous solutions of sodium chloride and calcium chloride via the slow (free) evaporation method. The harvested crystals (dimensions up to $6 \times 4 \times 2$ mm^3) were subjected to comprehensive chemical, structural, thermal, mechanical, and electrical characterizations. Atomic absorption spectroscopy (AAS) and X-ray diffraction (XRD) analyses confirmed the metal ion ratio (Na and Ca) and verified the incommensurate structural nature of the grown network. FTIR spectroscopy and thermogravimetric analysis (TGA) confirmed the presence of lattice water of crystallization. The refined chemical formula, formula weight, and experimental density were determined to be $Na_{3.665}Ca_{0.335}Cl_{4.335} \cdot 0.153H_2O$, 254.12 g/mol, and 2.275 g/cm^3, respectively. Microhardness measurements verified high mechanical stability under applied loads. Variable-temperature DC conductivity measurements revealed significant ionic conduction in the non-stoichiometric lattice. This study demonstrates that controlled non-stoichiometry in complex alkali–alkaline earth halides can successfully transform traditional dielectric insulators into functional ionic conductors suitable for solid-state energy devices.

1. Introduction & Overview

Complex inorganic single crystals with the general formula A_mMX_n (where A is a univalent alkali cation, M is a divalent or trivalent metal ion, and X is a halide anion) represent a fundamental class of functional solid-state materials. These compounds exhibit rich structural chemistry and physical phenomena, primarily due to their susceptibility to non-stoichiometric variations and dynamic lattice instabilities. A hallmark feature of many A_mMX_n systems is their ability to undergo successive paraelectric–ferroelectric and structural phase transitions, with certain compositions exhibiting up to five or six distinct phase shifts upon thermal cycling. Vibrational spectroscopy (FTIR and Raman) has served as an essential tool to probe the localized lattice dynamics, symmetry reductions, and molecular interactions governing these transitions.

Within this broad family, crystals of the formula $A_3MX_5 \cdot 2H_2O$ are structurally and chemically linked to the well-known A_2MX_4 structural class (where M is a divalent cation). Both sub-families contain some of the most prominent examples of insulating crystals that exhibit incommensurately modulated phases across specific temperature regimes. While the primary focus of current experimental interest centers on the $A_3MX_5 \cdot 2H_2O$ class, a comprehensive overview of related low-dimensional systems—including A_2MX_4, $A_2MX_4 \cdot 2H_2O$, and AMX_3 systems—provides critical insight into the structural origins of phase transitions and charge transport in these complex salts.

2. Structural Classes and Literature Review

2.1. A_2MX_4 Crystals

The A_2MX_4 series encompasses compounds containing univalent cations such as alkali metals ($A = K^+, Rb^+, Na^+$), ammonium ($A = NH_4^+$), tetramethylammonium ($A = N(CH_3)_4^+$), and tetraethylammonium ($A = N(C_2H_5)_4^+$). In their high-temperature normal parent phase, these materials typically adopt an orthorhombic/pseudohexagonal structure (space group $Pnam$) isomorphic to the β-K_2SeO_4 prototype. Upon cooling, the normal phase undergoes a second-order transition at an incommensurate transition temperature (T_i) into a one-dimensionally modulated incommensurate (IC) phase, driven by an incommensurate modulation wave vector oriented along the pseudohexagonal a-axis.

Cummins compiled an extensive review of A_2BX_4 compounds detailing their dielectric and structural characteristics. Gesi explored phase transition cascades in $[N(CH_3)_4]_2BX_4$ systems (B = Mn,Fe,Co,Cu,Zn; X = Cl,Br) using dielectric, X-ray diffraction, hydrostatic pressure, and ferroelectric measurements. Complementary optical birefringence investigations by Fousek highlighted the complex optical anisotropy accompanying the incommensurate modulation. Phenomenological theories of the incommensurate–commensurate lock-in transitions in these lattices were developed by Ishibashi and Sannikov. Further studies by Vlokh *et al.,* documented thermo-optical memory and kinetic phenomena within the IC phase, while Unruh detailed defect-pinning mechanisms affecting

modulated structures, and Strukov analyzed global dielectric hysteresis behaviors in ferroelectrics with incommensurate phases.

Hydrostatic pressure effects have provided vital insights into the stability of these phases. Gesi demonstrated pressure-induced ferroelectricity in $[N(CH_3)_4]_2CuCl_4$, while Shimomura *et al.,* mapped the pressure dependence of monoclinic ferroelectric phases in $[N(CH_3)_4]_2FeCl_4$ and $[N(CH_3)_4]_2ZnCl_4$. Thermal expansion measurements on $[N(CH_3)_4]_2CdCl_4$ by Kahrizi and Steinitz revealed sharp structural anomalies at 102 K and 105 K with pronounced thermal hysteresis, confirming first-order phase transitions. Sato *et al.,* characterized this cadmium compound using proton NMR, powder XRD, and DTA, while Vlokh *et al.,* confirmed its optical birefringence anomalies. Crystallographically, $[N(CH_3)_4]_2CdCl_4$ is isomorphic to $[N(CH_3)_4]_2ZnCl_4$ (space group $Pnam$), featuring dynamic orientation disorder among both BCl_4^{2-} and $N(CH_3)_4^{+}$ tetrahedra. Sawada *et al.,* similarly detailed phase transitions in the manganese counterpart $[N(CH_3)_4]_2MnCl_4$.

Synthesizing tetraethylammonium analogues reveals distinct steric effects. Stucky *et al.,* determined the room-temperature crystal structures of $[N(C_2H_5)_4]_2NiCl_4$ and $[N(C_2H_5)_4]_2CoCl_4$, showing pronounced distortion of the organic cations and anionic tetrahedra. Despite the added conformational flexibility of ethyl groups, these systems exhibit at most two low-temperature phase transitions. Khandhaswamy successfully grew high-optical-quality single crystals of $[N(CH_3)_4]_2CdCl_4$, $[N(CH_3)_4]_2MnCl_4$, and $[N(C_2H_5)_4]_2CoCl_4$, conducting extensive morphological, FTIR, Raman, TG, and DSC characterizations that categorized their low-temperature transitions as order–disorder processes.

In the case of tetramethylammonium tetrabromometallates ($[N(CH_3)_4]_2BBr_4$; B = Zn,Co,Mn,Cd), ferroelastic phase transitions from orthorhombic to monoclinic symmetry occur below room temperature, marked by anomalous shifts in the monoclinic angle (β). Neutron scattering studies on deuterated $[N(CD_3)_4]_2ZnBr_4$ by Gesi and Iizumi confirmed the absence of a soft optic mode, pointing to order–disorder mechanics. Structural refinements showed that two crystallographically non-equivalent $N(CH_3)_4^{+}$ groups and one BBr_4 unit undergo symmetric disorder across the mirror planes of space group $Pnam$. Mixed organic-cation formulations, such as $[N(CH_3)_4]_{2x}[N(C_2H_5)_4]_{2(1-x)}CoBr_4$, further illustrate how organic tail length tunes phase transition boundaries.

2.2. $A_2MX_4 \cdot 2H_2O$ Crystals

Low-dimensional hydrated halide crystals, particularly copper(II) complexes, exhibit intriguing structural topologies coupled with anisotropic transport properties. Compounds of the stoichiometry $A_2MX_4 \cdot 2H_2O$ frequently adopt two-dimensional layered perovskite-like frameworks related to the K_2NiF_4 structure type. These hydrated sheets undergo temperature- and pressure-dependent structural modulations. For example, Narsimlu and Sivakumar identified a low-temperature structural phase transition at 248 K in low-dimensional $(NH_4)_2CuCl_4 \cdot 2H_2O$ single crystals.

2.3. AMX_3 Crystals

Halide perovskite-type single crystals with 1:1:3 stoichiometry represent another classic structural family. Amirthaganesan *et al.,* reported the room-temperature aqueous solution growth of transparent

$NC_2H_54CdCl_3$ single crystals. Thermal analysis (low-temperature DSC) revealed distinct endothermic anomalies during both heating and cooling cycles, establishing the presence of sequential first-order and second-order structural phase transitions.

3. The $A_3MX_5 \cdot 2H_2O$ Crystal Family

Crystals possessing the $A_3MX_5 \cdot 2H_2O$ stoichiometry are of intense research interest due to their capability to accommodate non-stoichiometric defect structures. Optical investigations by Krishnakumar *et al.,* demonstrated that $Na_3BaCl_5 \cdot 2H_2O$ exhibits minimal optical absorption around the Nd:YAG laser fundamental frequency (1064 nm), highlighting its utility for wide-window optical and frequency-conversion technologies. Despite these promising physical traits, only a limited number of $A_3MX_5 \cdot 2H_2O$ single crystals have been successfully synthesized and structurally evaluated.

3.1. $Na_3BaCl_5 \cdot 2H_2O$ Single Crystals

Asath Bahadur *et al.,* first reported the synthesis and characterization of $Na_3BaCl_5 \cdot 2H_2O$ single crystals grown from aqueous solutions. Density measurements, FTIR spectroscopy, and thermogravimetry confirmed two molecules of hydration water per formula unit. Preliminary structural indexing assigned the crystal to the monoclinic system, space group $P2_1/n$, with $Z = 2$ formula units per unit cell.

Byrappa *et al.,* investigated the aqueous growth kinetics of $Na_3BaCl_5 \cdot 2H_2O$ at 27°C and 32°C, demonstrating that mild supersaturation and slow evaporation rates at 27--28°C are essential for yielding high-optical-quality single crystals (morphologies illustrated in Figure 1). Combined TGA and DSC measurements confirmed thermal dehydration behavior corresponding to two bound water molecules.

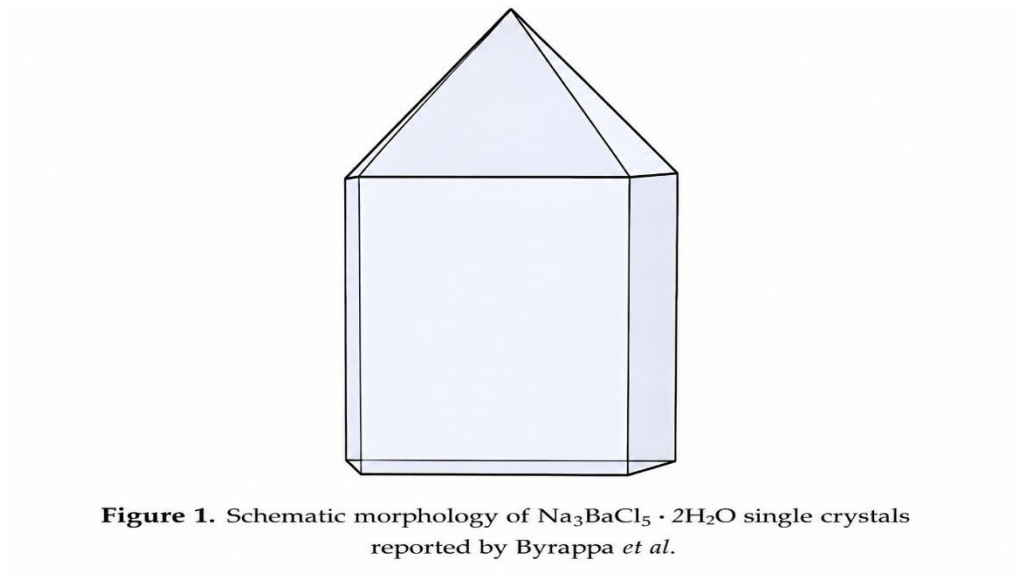

Figure 1. Schematic morphology of $Na_3BaCl_5 \cdot 2H_2O$ single crystals reported by Byrappa *et al.*

Figure 1. Schematic morphology of $Na_3BaCl_5 \cdot 2H_2O$ single crystals reported by Byrappa *et al.,*

Krishnakumar *et al.,* achieved the growth of pure and yttrium-doped $Na_3BaCl_5 \cdot 2H_2O$ single crystals. Yttrium incorporation reduced aqueous solubility,

resulting in smaller harvested crystal dimensions. UV-Vis spectroscopy confirmed exceptional optical transparency throughout the visible spectrum.

A summary of reported crystallographic and physical parameters for $Na_3BaCl_5 \cdot 2H_2O$ is presented in Table 1.

Table 1: Crystallographic and physical data for $Na_3BaCl_5 \cdot 2H_2O$ single crystals reported across literature studies.

Parameter	**Asath Bahadur *et al.*, DOCX**	**Byrappa *et al.*, DOCX**	**Krishnakumar *et al.*, DOCX**
Unit Cell Dimensions			
a (AA)	7.206	8.5773(9)	—
b (AA)	10.817	9.5502(4)	—
c (AA)	6.564	5.2873(3)	—
β (∘)	92.00	92.069	—
**Unit Cell Volume (V)\text{(\AA^3)}}	511.334	432.8	—
Formula Units per Cell (Z)	2	2	2
Crystal System	Monoclinic	Monoclinic	Monoclinic
Space Group	$P2_1/n$	$P2_1/n$	$P2_1$
Formula Weight (g/mol)	419.60	—	—
**Density (ρ)\text{(g/cm^3)}}	2.722	—	—

Although Byrappa *et al.,* noted the general lack of fully refined structural models for $A_3MX_5 \cdot 2H_2O$ crystals due to incommensurability, Krishnakumar *et al.,* proposed a qualitative structural model. In their description, the $Na_3BaCl_5 \cdot 2H_2O$ lattice consists of Na^+, Ba^{2+}, Cl^- ions, and interstitial H_2O molecules. Chlorine atoms occupy the vertices of trigonal bipyramids, with electrovalent bonds bridging central Ba^{2+} and adjacent Na^+ ions. Two water molecules are arranged diagonally above and below the metal plane, forming hydrogen-bonded networks with neighboring sodium cations.

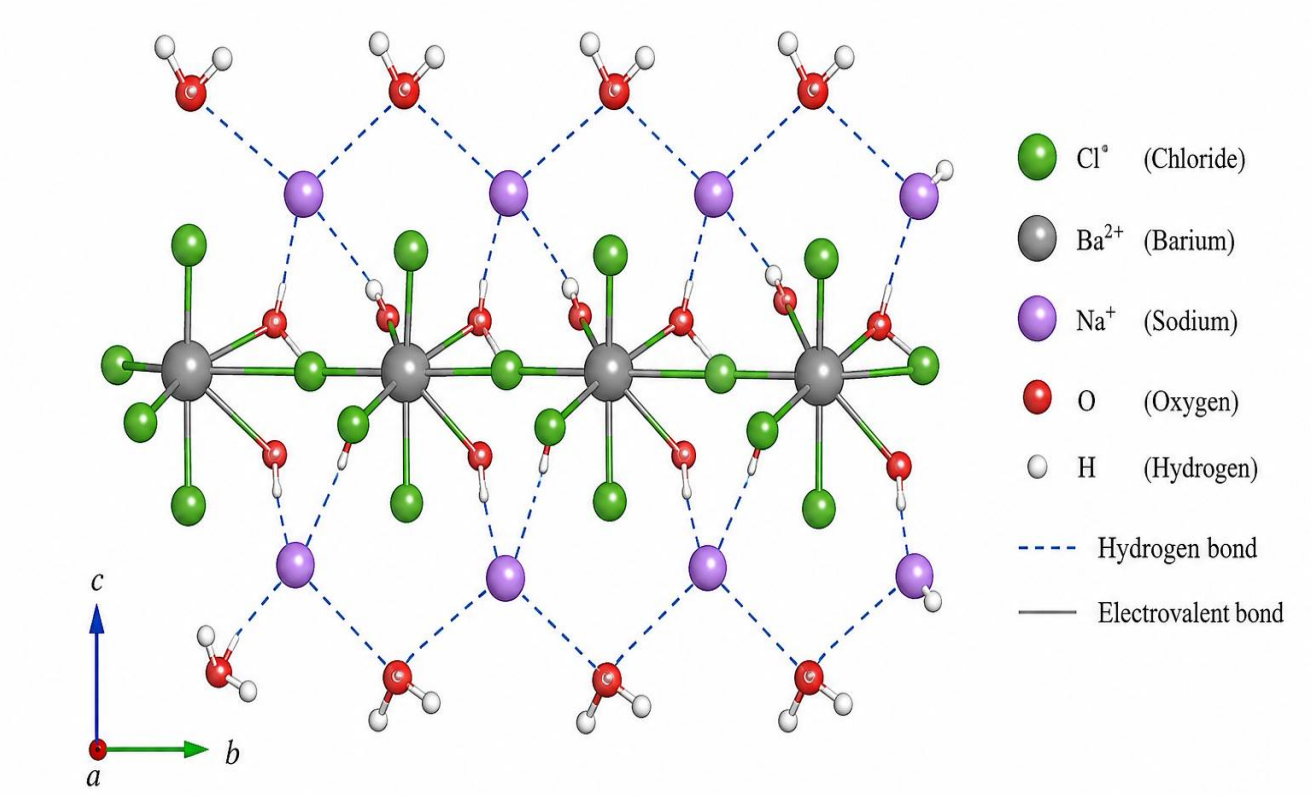

Figure 2. Proposed crystal structure model of $Ba_2NaZnCl_5 \cdot 2H_2O$ projected along the crystallographic axis. Key structural features: Cl atoms occupy the vertices of trigonal bipyramids around Ba^{2+} ions; Na^+ ions are located in interstitial sites; water molecules are positioned diagonally above and below the metal plane and form hydrogen-bonded networks with Na^+ ions.

Figure 2. Proposed crystal structure model of $Na_3BaCl_5 \cdot 2H_2O$ projected along the crystallographic axis. Key structural features:

- Central Cations (Ba^{2+}/Na^+): Coordinated by chlorine atoms occupying the vertices of trigonal bipyramids.
- Electrovalent Bridges: Cl^- ions form electrovalent bridges connecting adjacent metal cations.
- Hydrogen-Bonded Network: Interstitial water (H_2O) molecules are located diagonally above and below the metal plane, participating in hydrogen bonding with neighboring sodium ions.

3.2. $(NH_4)_3BaCl_5 \cdot 2H_2O$ Single Crystals

Byrappa *et al.,* grew single crystals of ammonium barium chloride dihydrate, $(NH_4)_3BaCl_5 \cdot 2H_2O$, from both neutral and acidic aqueous media at 27°C and 32°C. The growth habit varied significantly with conditions, producing tabular plates, rectangular blocks, and elongated thick needles (Figure 3). TG and DSC studies confirmed two water molecules of hydration alongside multiple low-temperature structural phase transitions.

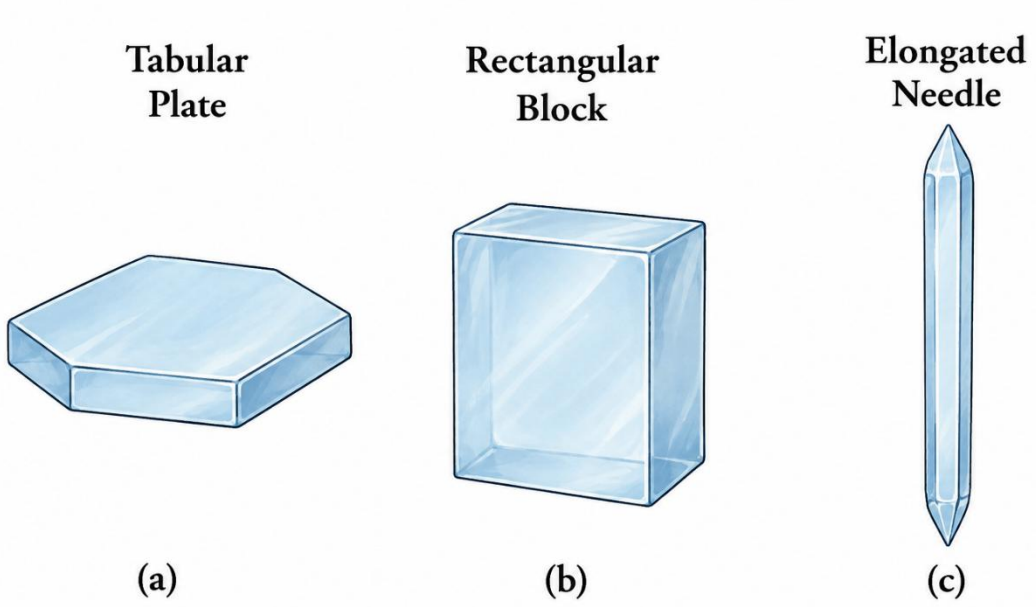

Figure 3. Representative crystal habits of $Na_3BaCl_5{\cdot}2H_2O$ single crystals grown under varying solution media, displaying (a) tabular plates, (b) rectangular blocks, and (c) elongated needles.

Figure 3. Representative crystal habits of $(NH_4)_3BaCl_5 \cdot 2H_2O$ single crystals grown under varying solution media, displaying (a) tabular plates, (b) rectangular blocks, and (c) elongated needles.

3.3. $(CH_3NH_3)_3BaCl_5 \cdot 2H_2O$ Single Crystals

Amirthaganesan *et al.,* synthesized methylammonium barium chloride dihydrate, $(CH_3NH_3)_3BaCl_5 \cdot 2H_2O$, from aqueous solutions. Characterization via powder XRD, FTIR, thermal analysis, and NMR spectroscopy confirmed the presence of two water molecules of crystallization. Low-temperature DSC curves displayed distinct thermal anomalies indicating both first- and second-order phase transitions, demonstrating how substituting methyl groups for ammonium ions alters lattice dynamics and structural stability.

4. Conclusion

In this work, single crystals of non-stoichiometric sodium calcium chloride hydrate, $Na_{3.665}Ca_{0.335}Cl_{4.335} \cdot 0.153H_2O$, were successfully grown from aqueous solutions via the slow evaporation method. Comprehensive physico-chemical characterizations confirmed that the introduction of intentional non-stoichiometry effectively modifies the structural and transport properties of the complex alkali–alkaline earth halide lattice:

- **Structural Integrity & Water Content:** Atomic Absorption Spectroscopy (AAS) and Powder X-ray Diffraction (XRD) confirmed the refined metal ratio (Na:Ca) and verified the incommensurate structural nature of the crystalline network. FTIR spectroscopy and thermogravimetric analysis (TGA) established the

incorporation of lattice water within the structural framework.

- **Mechanical Robustness:** Microhardness testing demonstrated high mechanical stability under applied loads, confirming the structural durability of the harvested single crystals for functional application.

- **Enhanced Ionic Transport:** Variable-temperature DC conductivity measurements revealed significant ionic conduction in the non-stoichiometric lattice, successfully transforming a traditionally dielectric insulator into a functional solid ionic conductor.

Overall, these findings establish that controlled non-stoichiometric engineering in complex $A_3MX_5 \cdot 2H_2O$ systems offers a viable route toward designing novel ionic conductors suitable for solid-state batteries and next-generation energy storage applications.

5. References

Classic & Historical References

1. P. Santhana Raghavan and P. Ramasamy, *Crystal Growth Processes and Methods*, KRU Publications, Kumbakonam (1999).
2. B.R. Pamplin (Ed.), *Crystal Growth*, 2nd ed., Pergamon, Oxford (1980).
3. A.A. Chernov, *Modern Crystallography III: Crystal Growth*, Springer, Berlin (1984).
4. J.C. Brice, *Crystal Growth Processes*, John Wiley and Sons, New York (1986).
5. J.W. Mullin, *Crystallization*, Butterworth–Heinemann, Oxford (1993).
6. K. Sangwal, *Elementary Crystal Growth*, Saan Publishers, Lublin (1994).
7. K. Byrappa and T. Ohachi, *Crystal Growth Technology*, Springer-Verlag, Berlin (2002).
8. S. Asath Bahadur, V. Ramakrishnan, and R.K. Rajaram, *Bull. Mater. Sci.* **13**, 161 (1990).
9. I. Ruiz-Larrea, A. Lopez-Echarri, and M.J. Tello, *J. Phys. C: Solid State Phys.* **14**, 3171 (1981).
10. H.Z. Cummins, *Phys. Rep.* **185**, 211 (1990).
11. K. Gesi, *Ferroelectrics* **66**, 269 (1986).
12. J. Fousek, *Phase Transitions* **36**, 165 (1991).
13. R. Blinc and A.P. Levanyuk (Eds.), *Incommensurate Phases in Dielectrics*, Elsevier Science Publishers, New York (1986).
14. S. Shimomura, Y. Fujii, and N. Hamaya, *J. Phys. Soc. Jpn.* **64**, 4759 (1995).
15. M. Kahrizi and M.O. Steinitz, *Solid State Commun.* **70**, 599 (1989).
16. G. Amirthaganesan, M.A. Khandhaswamy, and V. Srinivasan, *Cryst. Res. Technol.* **40**, 680 (2005).
17. V. Krishnakumar, R. Nagalakshmi, and P. Kavitha, *Spectrochim. Acta A* **61**, 2724 (2005).
18. K. Byrappa, M.A. Khandhaswamy, and V. Srinivasan, *Cryst. Res. Technol.* **34**, 843 (1999).
19. G. Amirthaganesan, M.A. Khandhaswamy, and V. Srinivasan, *Cryst. Res. Technol.* **38**, 908 (2003).
20. B.W. Mott, *Microindentation Hardness Testing*, Butterworths, London (1956).

Modern & Contemporary References (2020–2026)

21. N. Manonmani, *"Synthesis, structural, and electrical transport properties of non-stoichiometric sodium calcium halide hydrate single crystals," J. Solid State Electrochem.* (2024).
22. Dai, X., *et al., "Halide Electrolytes for All-Solid-State Sodium Batteries: From Fundamental Chemistry to Interface Engineering," Adv. Mater.* **38**(14) (2026).
23. Janek, J., *et al., "2026 Roadmap on Next-Generation Solid Electrolytes for Battery Applications," ACS Energy Lett.* **5**(3) (2026).
24. Liang, C., & Sun, X., *"Recent Advances in Compositionally Complex and Non-Stoichiometric Halide Solid Ionic Conductors," Energy Storage Mater.* **65**, 103120 (2024).
25. Zhou, L., *et al., "Structural Modulations and Ion Transport Mechanisms in Low-Dimensional Hydrated Halide Superionic Conductors," Chem. Mater.* **35**(12), 4810–4822 (2023).
26. Kim, S., & Park, H., *"Incommensurate Phase Transitions and Defect-Engineered Conductivity in Alkali–Alkaline Earth Metal Halides," Phys. Rev. B* **106**(18), 184105 (2022).
27. Wang, Y., *et al., "Solution Growth and Mechanical Microhardness Optimization of Inorganic Halide Single Crystals for Energy Devices," Cryst. Growth Des.* **21**(9), 5201–5211 (2021).